



Effects of loading rate and peak load on nanoindentation creep behavior of DD407 Ni-base single crystal superalloy

Zhen-nan ZHANG¹, Yun-li LI², Wen-ping WU^{1,3}

1. Department of Engineering Mechanics, School of Civil Engineering, Wuhan University, Wuhan 430072, China;

2. School of Civil Engineering and Architecture, Wuhan Institute of Technology, Wuhan 430074, China;

3. State Key Laboratory of Water Resources & Hydropower Engineering Science,
Wuhan University, Wuhan 430072, China

Received 7 January 2021; accepted 26 July 2021

Abstract: Nanoindentation experiments were conducted under loading rates of 500–6000 $\mu\text{N/s}$ and applied peak loads of 4000–12000 μN to measure the creep behavior of DD407 Ni-base single crystal superalloy at room temperature. Experimental results demonstrated that DD407 Ni-base single crystal superalloy had a good creep resistance, but its creep properties were sensitive to the loading rate and peak load. The fitting creep parameters significantly increased with increasing loading rate and peak load based on the Findley's model, and the corresponding creep mechanism was governed by dislocation based on the calculation of creep stress exponent. During nanoindentation creep tests, it was found that the hardness and reduced modulus decreased with increasing the loading rate and peak load, and through a dimensionless analysis, it was also noted that the effect of the dimensionless loading rate was stronger than that of dimensionless peak load on the creep properties.

Key words: DD407 Ni-base single crystal superalloy; nanoindentation; Findley's model; creep; stress exponent

1 Introduction

Ni-base single-crystal superalloys have been widely used as crucial materials for turbine blades in aero-engines, due to corresponding superior mechanical strength and excellent creep resistance [1]. Creep-induced failure is an important lifetime limiting failure mode in Ni-base single-crystal superalloys applications [2,3]. Usually, these alloys are produced as single crystals for increased creep resistance [4], among which, the newly developed DD407 single crystal Ni-base superalloy presents good comprehensive mechanical properties. Consequently, to better understand the creep behaviors of Ni-base single crystal superalloy under different loading conditions, several experiments

were conducted for the DD407 Ni-base single crystal superalloy in this study.

As a standard technique to determine the creep behavior of engineering materials, the uniaxial tension test has constituted the main utilized method for creep research in recent years. Based on this technique, WOLLGRAMM et al [5,6] determined that the stress dependence of creep rates could be well described by the power law in an ERBO1 single crystal superalloy. SHI et al [7] predicted the creep lifetime of a directionally solidified (DS) superalloy at elevated temperatures. SUN et al [8] studied the effect of film-hole configuration on the creep rupture behavior of DD6 nickel-based single crystal superalloys. Adversely, many uniaxial creep tests were required for each specimen that could only yield one data point,

Corresponding author: Yun-li LI, Tel: +86-27-68775496, E-mail: liyunli@wit.edu.cn;

Wen-ping WU, Tel: +86-27-68775496, E-mail: wpwu@whu.edu.cn

DOI: 10.1016/S1003-6326(21)65788-6

1003-6326/© 2022 The Nonferrous Metals Society of China. Published by Elsevier Ltd & Science Press

resulting in the heavy consumption of materials. Moreover, in certain cases, the results obtained from the standard uniaxial creep specimens did not always represent the mechanical properties of the serviced materials. As an example, for the turbine blades that had been serviced for a certain period, the corresponding creep properties were required to be measured by the standard uniaxial creep test; however, it is not suitable for thin films, coatings or other low-sized material structures. It must be noted that the mechanical properties of these widely employed low-sized material systems can be quite different compared to their bulk counterpart [9,10]. Therefore, the effective measurement of their creep properties imposed a significant challenge in the cases where the conventional uniaxial method was no longer suitable.

Nanoindentation provided an effective choice to achieve this goal and determines the mechanical properties of a material in the sub-micron or nanometer scales. Nanoindentation technique was first proposed by DOERNER and NIX [11] and further developed by OLIVER and PHARR [12,13]. The mechanical information can be derived from both recorded depth and measured applied load. The creep behavior was measured through the indenter driving into the material until a certain loading force was reached. This force was consequently retained constant and the sample indentation was measured as a function of time. In comparison to macroscopic mechanical testing (such as uniaxial tension), nanoindentation exhibits several attractive advantages in the mechanical property determination of materials, and this technique has been widely applied to studying the creep behavior of metallic alloys. For instance, HASEEB et al [14] investigated the nanoindentation creep on the copper alloys with different doping components. MA et al [15] studied the creep behavior of two different structural states of a ferroalloy through nanoindentation. A bridge between nanoindentation creep and uniaxial creep for aluminum of the commercial purity was established by PHANI and OLIVER [16]. Nevertheless, only a few studies regarding the creep behavior of Ni- base single crystal superalloy with nanoindentation have been carried out [17], there was a lack of in-depth understanding of the creep behavior and related influencing factors during nanoindentation.

In this work, the effects of loading rate and applied peak load on the nanoindentation creep behavior of the DD407 Ni-base single crystal superalloy at room temperature were highlighted. The loading rates (500–6000 $\mu\text{N/s}$) and the applied peak loads (4000–12000 μN) were selected on account of certain successful nanoindentation creep experiments [18–21]. All results were analyzed in terms of the Findley's model [22] which could quantitatively describe the creep curves, and the creep stress exponents were calculated to analyze the creep mechanism. Based on the analysis of the results under different testing conditions, the relationship between load levels and creep behaviors in nanometer-scale was explored, to provide a new way of thinking for the follow-up studies and contribute to the working condition optimization for blades in aero-engines.

2 Experimental

2.1 Materials and preparation

The studied single-crystal superalloy was DD407, as presented in Fig. 1(a), for nano-indentation testing. Figure 1(b) presented the DD407 microstructure, which displayed a near-unimodal distribution of the submicron cuboidal γ' precipitates within γ matrix from the SEM image.

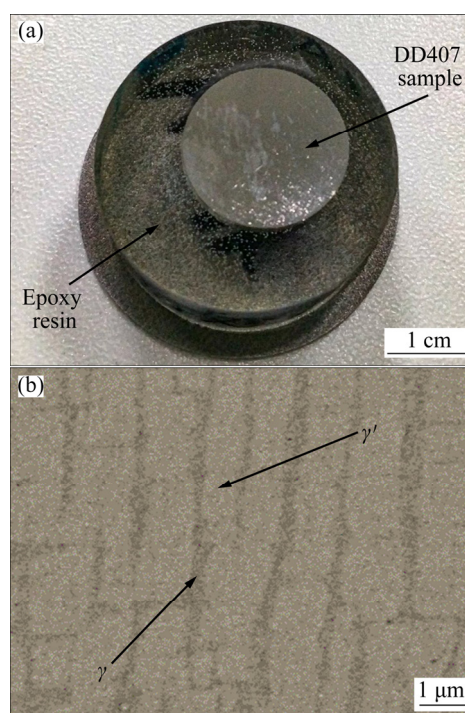


Fig. 1 Treated DD407 sample embedded in epoxy resin (a), and SEM image of γ/γ' microstructure of DD407 (b)

The chemical components of DD407 were presented in Table 1 [23,24]. Before nanoindentation testing, certain preparations were made as follows: (1) The samples were embedded in epoxy resin and dried for 24 h; (2) The samples were polished with a Buehler polishing machine with sandpapers of 800[#] and 2500[#] grit. Consequently, 3, 1 and 0.05 μm of a polishing slurry were used until the sample surfaces were mirror cleaned. During experimentation, each sample was tested 9 times.

Table 1 Chemical components of DD407 (wt.%)

Cr	Al	W	Mo	Co	Ti	Ta	Ni
8.00	6.00	5.00	2.25	5.50	2.00	3.50	Residue

2.2 Nanoindentation

Nanoindentation creep testing was conducted at room temperature of 22 °C on Hysitron Ti-950 TriboIndenter (Hysitron Inc., USA) equipped with a spherical diamond indenter, with a tip radius of 5.28 μm upon the standard aluminum sample calibration, as shown in Fig. 2. Note that a spherical

tip was better than sharp tips (such as Berkovich and Vickers) owing to relatively low stress concentration and large indentation/process zone on the contact surface [25].

Two sets of nanoindentation experimental schemes were designed: (1) Loading rate-sensitive experiments: The peak load remained unchanged at 6000 μN and the holding time was 100 s, but the loading rate varied with different constant values of 500, 1000, 2000, 4000 and 6000 $\mu\text{N/s}$, respectively; (2) Peak load sensitive experiments: The holding time and the loading rate were maintained at 100 s and 1000 $\mu\text{N/s}$, but the peak load varied from 4000 to 12000 μN with an increment of 2000 μN for each group of tests. In addition, every point was selected in the imaging pattern, which was similar to in-situ testing, to reduce the error caused by the surface difference.

A typical load (P) versus time (t) curve of nanoindentation creep test (peak load 12000 μN , loading rate 1000 $\mu\text{N/s}$, holding time 100 s) is shown in Fig. 2(b). This curve can well describe the loading mode of nanoindentation. Other loading modes are similar to this one.

3 Results and discussion

3.1 Nanoindentation creep analysis

Nanoindentation constitutes the diamond indenter pressing into the testing material with a certain geometric shape. For the spherical indenter, the directions of the stresses varied with each point in the region of action due to the geometry inhomogeneity. Therefore, it was necessary to use the equivalent method to obtain the stress value through the indentation testing measurements. The model can be simplified as a rigid indenter, and pressed into a semi-infinite volume. During the nanoindentation creep testing, the equivalent stress (σ) can be described as [12]

$$\sigma = k_1 H = k_1 \frac{P}{A_c} \quad (1)$$

$$A_c = \pi h_c (2R - h_c) \quad (2)$$

$$h_c = h - \frac{\varepsilon P}{S} \quad (3)$$

where k_1 is a constant, H and P represent the hardness and the applied load, respectively. Usually, the value of k_1 is 1/3, and A_c represents the contact projection area. R is the radius of the indenter; h_c is

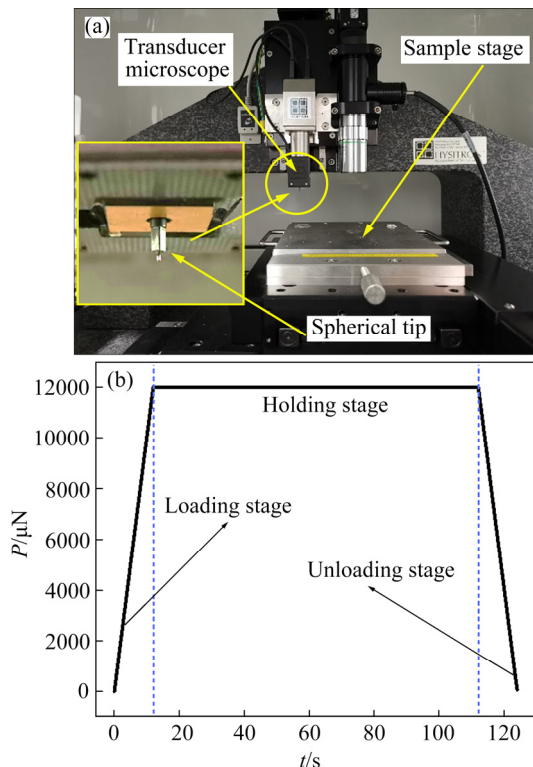


Fig. 2 Hysitron TI-950 TriboIndenter equipment (a), and typical load versus time curve of nanoindentation creep test including loading stage, holding stage and unloading stage (b)

the contact depth of the indenter and initial surface, which can be calculated according to the Oliver–Pharr method [12,13]; h is the total displacement at random time during holding period; ε is the geometric constant, usually $\varepsilon=0.75$ for spherical diamond indenter; S is the stiffness.

Through Eqs. (2) and (3) substitution into Eq. (1), the relationship between the stress (σ) and the total displacement (h) is expressed as follows:

$$\sigma = \frac{P}{3\pi(h - 0.75\frac{P}{S}) \left[2R - \left(h - 0.75\frac{P}{S} \right) \right]} \quad (4)$$

The strain rate $\dot{\varepsilon}$ is defined as the instantaneous rate of the indenter, which is the ratio of dh/dt to the instantaneous depth h .

$$\dot{\varepsilon} = k_2 \left(\frac{dh}{dt} \right) \frac{1}{h} \quad (5)$$

where k_2 is a constant and equals 1 in these experiments. According to the exponential creep law, the relationship between $\dot{\varepsilon}$ and σ is established upon the power law equation:

$$\dot{\varepsilon} = A_0 \sigma^n \quad (6)$$

where A_0 is the material constant; n is the creep stress exponent that can reflect the mechanism of creep, as presented in Table 2 [26–28]. This mechanism can be defined by

$$n = \frac{\partial(\ln \dot{\varepsilon})}{\partial(\ln \sigma)} \quad (7)$$

Table 2 Creep stress exponent and corresponding creep mechanism

Stress exponent	Mechanism
1–2	Grain boundary diffusion control or lattice diffusion control
≥ 3	Dislocation control

3.2 Creep behavior at various loading rates

Figure 3(a) showed the representative ($P-h$) curves of DD407 samples corresponding to five test loading rates (500, 1000, 2000, 4000, 6000 $\mu\text{N/s}$). The applying peak load was 6000 μN under a specific holding time of 100 s. Figure 3(b) illustrated the variations in creep depth of the indenter tip into the sample surface with holding time for the DD407 Ni-base single crystal superalloy at different loading rates. The starting

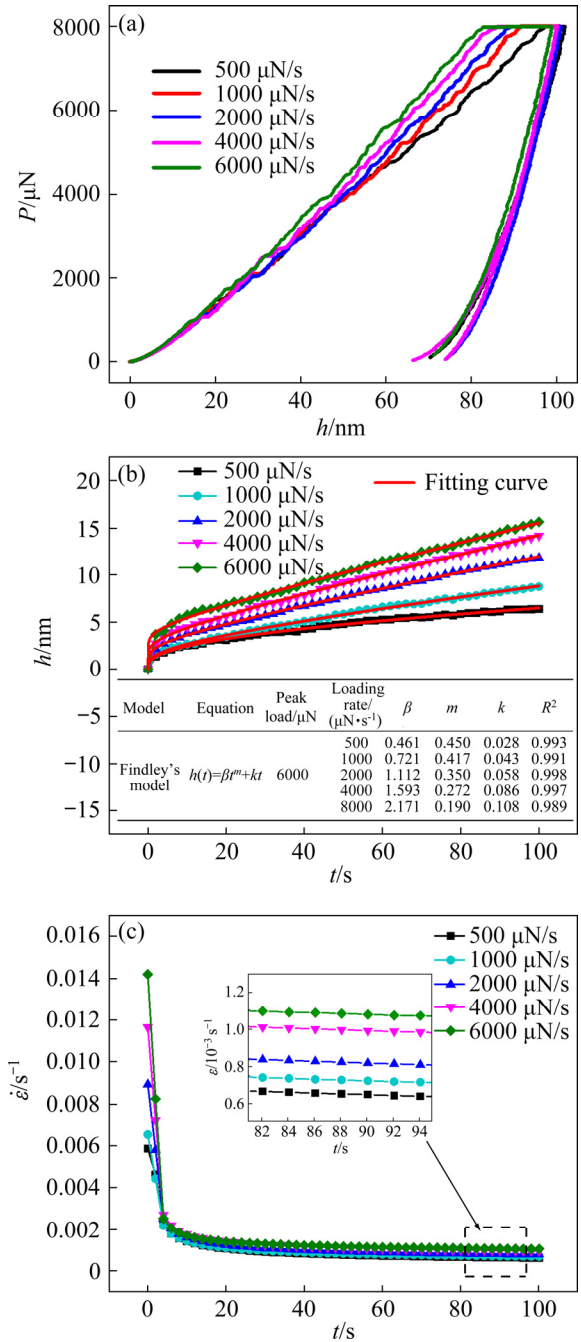


Fig. 3 Typical loading rate-sensitive $P-h$ curves (a), typical Findley's creep curves and fitting parameters (b), and variations in creep strain rate with holding time of 100 s (c) for DD407 Ni-based single crystal superalloy under different loading rates

points of creep depth were aligned for comparison. Rate dependence of the creep displacement and the time relationship demonstrated that the maximum creep penetration depth continuously increased as the loading rate increased from 6.07 nm at 500 $\mu\text{N/s}$ to 15.94 nm at 6000 $\mu\text{N/s}$. This was consistent with

the observations from the bulk metallic glasses (BMGs) and the other crystalline materials [29].

To further analyze the creep behavior of DD407 through the Findley's model, the $h-t$ curve during holding time at constant indentation load can be expressed as [30]

$$h(t) = h_i + \beta(t - t_i)^m + kt \quad (8)$$

where h_i and t_i are the displacement and time at the beginning of the holding period, respectively, and the values were 0 by default in this study for better comparison. It can be simplified as follows:

$$h(t) = \beta t^m + kt \quad (9)$$

where β and m are related to the transient creep, and k represents the change of displacement, due to the steady-state creep. The experimental creep curves at different applied loading rates were fitted with the Findley's power law and illustrated in Fig. 3(b).

The creep displacement h increased as the applied loading rate increased. It was observed that the transient creep and steady-state creep displayed apparent distinctions. The Findley's model fitted very well with the current results with $R^2 \gg 0.99$. The results quantitatively demonstrated that the high loading rates corresponded to high valued parameters (β , m and k), suggesting that the creep of DD407 had a strong loading rate response. According to the nanoindentation creep research in polycrystalline Ni films, MA et al [21] found that under the minimum load rate, the strain rate was also the lowest. Therefore, it was necessary to maintain the load for a long duration. Also, the creep deformation might occur during this loading time. Consequently, the creep would decrease in the subsequent period. Another reason might be related to the research of GONG et al [29], when the indenter was pressed into the material, elastic deformation firstly occurred, then the elastic and plastic deformation simultaneously coexisted. Finally, the entire deformation became plastic deformation. For the alloys, the elastic deformation might spread faster compared to plastic deformation. When the sample was subjected to a high loading rate, plastic deformation might occur with delay for certain parts for the residual plastic deformation to be released during the holding time, resulting in a relatively large creep displacement. Furthermore, it also should be emphasized that although the spherical indenter was applied in the

present work (not a Berkovich indenter), a certain radius of curvature still existed, which led to stress concentration near the indenter tip, and thus increased the creep displacement to some extent. The results indicated that DD407 Ni-base single crystal superalloy had a good creep resistance at a lower loading rate though the creep displacement showed sensitivity to loading rate response in the nanoindentation experiment.

To further study the effect of loading rate on creep, the strain rate $\dot{\epsilon}$ was obtained based on Eq. (8) and it can be expressed as [31]

$$\dot{\epsilon} = \frac{dh}{dt} \frac{1}{h} = \left[\beta m (t - t_i)^{m-1} + k \right] \frac{1}{h} \quad (10)$$

During the loading period, the creep phenomenon occurred, while the strain rate from a high value gradually reached a relatively stable stage. The curves of creep rate versus holding time were plotted in Fig. 3(c). As it could be observed, every creep strain rate tended to saturate in the steady-state creep stage subsequently to 4 s. This was mainly attributed to certain features of work hardening during the steady-state creep process [32]. NORTHWOOD and SMITH [33] demonstrated that work hardening and recovery remarkably occurred during steady-state creeping in polycrystalline cadmium. This meant that the creep rate decreased with increasing time, becoming diminished. In order to compare the creep rates of the specimens, the values of stress and creep rate were defined following the initial sharp drop, as steady-state stress and creep rate. In this study, it could be observed that as the loading rate increased from 500 to 6000 $\mu\text{N/s}$, the steady creep rate changed from 6.8×10^{-4} to $1.1 \times 10^{-3} \text{ s}^{-1}$. RAMAN and BERRICHE [34] provided a possible reason to explain this phenomenon. The corresponding research demonstrated that the dislocation substructure formed in the head under different load strain rates, which would affect the subsequent creep behavior. Another possible explanation could be obtained from certain earlier studies [35–37], in which, it was observed that higher loading rates could lead to higher energy states. Apparently, higher energy might contribute to local heating, which would cause additional creep displacement. Although many possible theoretical explanations existed, the explanation for the dominant effect of the latter theory was still unclear. This also required

further study from the micro level. Accordingly, certain researchers suggested that the application of a high loading rate during testing constituted a feasible method to mitigate the creep effect [38]. Adversely, YANG et al [39] indicated that a quite high loading rate might induce a high-sized overshoot on the preset indentation load, which could further provoke the peak load instability. Therefore, the selection of an appropriate load rate must be paid full attention to the materials.

Figure 4(a) presented the logarithmic plots of strain rate versus stress extracted from typical creep curves at different loading rates. The transient creep (a_1) and steady-state creep (a_2) were fitted respectively. The slopes of the straight lines in Fig. 4(a) represented the stress exponent n , which could be extracted from Eq. (7). Figure 4(b) presented the average stress exponents and their error bars for several typical stress exponent lines at each loading rate. An apparent decrease in the steady-state creep stress exponent from 7.95 to 2.56 could be observed as the loading rate increased from 500 to 6000 $\mu\text{N/s}$. Compared to certain earlier experiments [16,40], the creep stress exponent under nanoindentation was a little higher than that under uniaxial creep, because higher stress/strain gradients and lower-sized indentation/process zones made the stress state under nanoindentation more complex and severer than the uniaxial state, the nanoindentation was capable of capturing highly localized effects [41,42].

In the nanoindentation creep analysis, a certain connection existed between the stress exponent and the deformation mechanisms [43]. The diffusion creep was dominant as the n value was below 1. The grain boundary sliding creep led to a value between 1 and 2. When the n value exceeded 3, the dislocation was mainly considered responsible for the creep behavior. Clearly, dislocation was dominant in these creep experiments, because all stress exponent values exceeded 3. The stress exponent decreased as the loading rate increased, whereas the mechanisms tended to be diffusion creep or grain boundary sliding creep when the loading rate was 6000 $\mu\text{N/s}$. One possible reason was that the high loading rate led to local heating, which caused the local temperature increase [44]. Higher temperature contributed to the diffusion acceleration of the atoms, while both the climb of

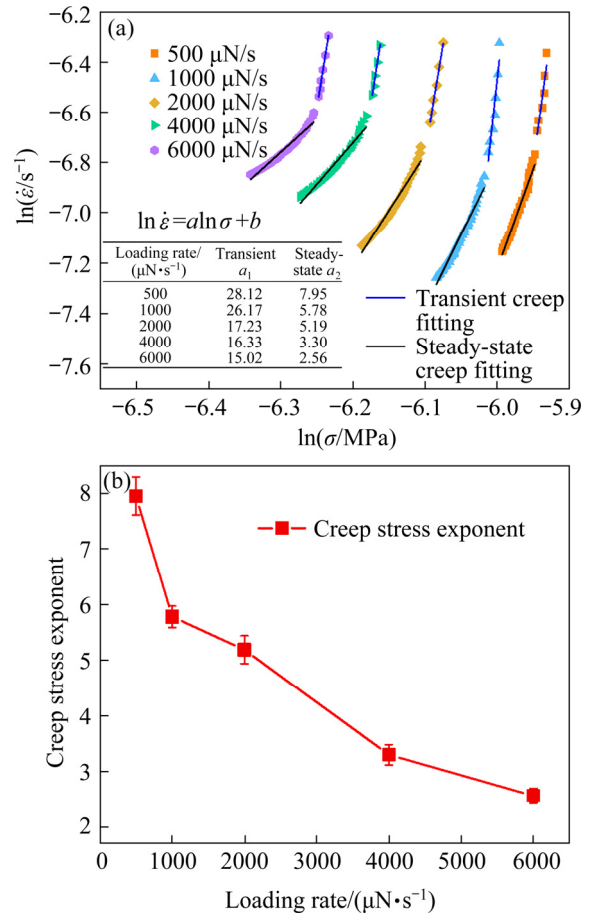


Fig. 4 Variation of stress exponent under different loading rates extracted from transient and steady-state creep stages (a), and average stress exponents and their error bars extracted from steady-state creep stage taken as valid n under different loading rates (b)

dislocations and the directional diffusion of vacancies contained atomic diffusion processes [45,46]. Therefore, as the loading rate increased, the creep stress exponent presented a decreasing trend.

Furthermore, variations in loading rate have also been associated with mechanical properties in DD407 such as hardness and reduced modulus. To verify the experimental results comprehensively, the values of hardness and resulted modulus were extracted by the Oliver–Pharr method [12] in Fig. 5. It can be seen that the higher loading rate corresponded to a lower reduced modulus (E_r) and H . They respectively reached the maximum of 1236.7 and 73.4 GPa at 500 $\mu\text{N/s}$, and the minimum of 811.3 and 50.4 GPa when the loading rate is 6000 $\mu\text{N/s}$. The main reason for this phenomenon is the scale effect of the nanoindentation test. When the indentation depth is deep, the bond energy of the material surface layer has little influence on the

measurement, which is mainly caused by the dislocation expansion inside the material. When the indentation depth is very small, there are only a few dislocations in the deformation zone. The bond energy of the atoms in the material surface layer plays a leading role in the measurement of the hardness [41].

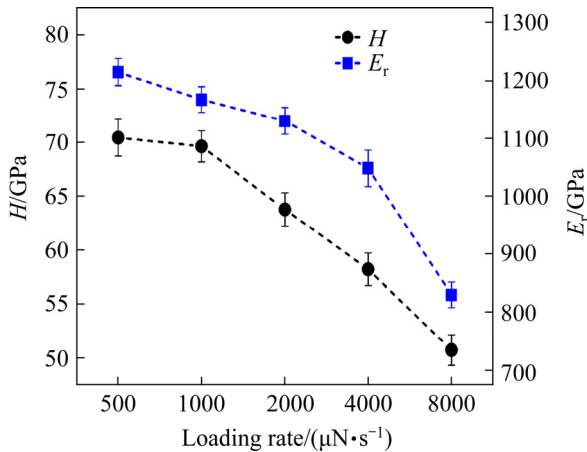


Fig. 5 Reduced modulus and hardness data for DD407 alloy under various loading rates

3.3 Creep behavior at various peak loads

Figure 6(a) showed the representative $P-h$ curves under different holding peak loads (4000, 6000, 8000, 10000, 12000 μN). The applying loading rate was 1000 $\mu\text{N}/\text{s}$ under a specific holding time of 100 s. Figure 6(b) presented the curves of creep displacement at each holding-time segment under the peak loads of 4000, 6000, 8000, 10000 and 12000 μN with a 1000 $\mu\text{N}/\text{s}$ loading/unloading rate and 100 s of holding time. As the peak load increased from 4000 to 12000 μN , the maximum creep depth during the holding period increased from 6.8 to 23.3 nm. Moreover, through the slope comparisons of the creep curves, it could be observed that the creep rates decreased gradually during the holding time, being easier to reach a steady-state under the lower peak load within the same period. This relationship was quantitatively described with the Findley's mode in Fig. 6(b). A similar result was obtained compared to the loading rate case. The result had a good fitting and all fitting parameters increased as the peak load increased. To better illustrate the creep effect, the fitted creep rate curves under different peak loads were extracted from Fig. 6(c). All curves decreased rapidly in the beginning, consequently becoming flat, but it was noticeable that the higher peak load

corresponded to a higher creep rate in the same time frame.

The stress exponents from typical creep curves were extracted as presented in Fig. 7(a). During nanoindentation creep testing, the creeping of the material was mainly related to the corresponding hardness and work hardening ability, whereas the creep stress exponent of the material could be obtained with a single measurement. Figure 7(b)

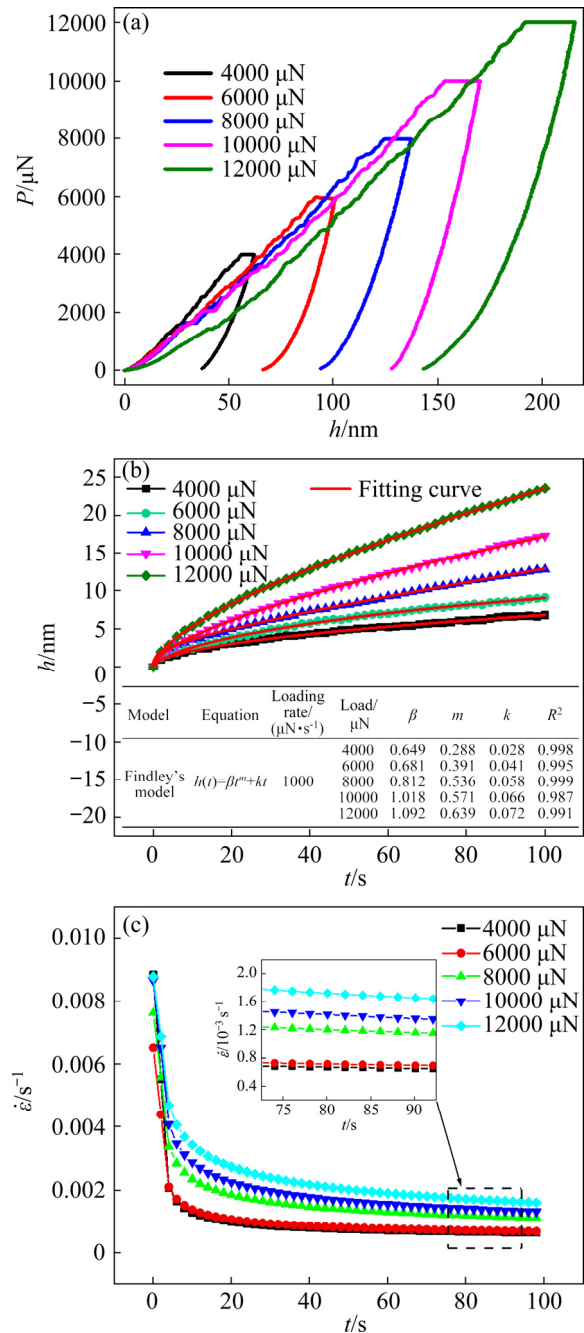


Fig. 6 Typical peak load-sensitive $P-h$ curves (a), typical Findley's creep curves and fitting (b), and variations in creep strain rate with holding time of 100 s for DD407 Ni-based single crystal superalloy under different peak loads (c)

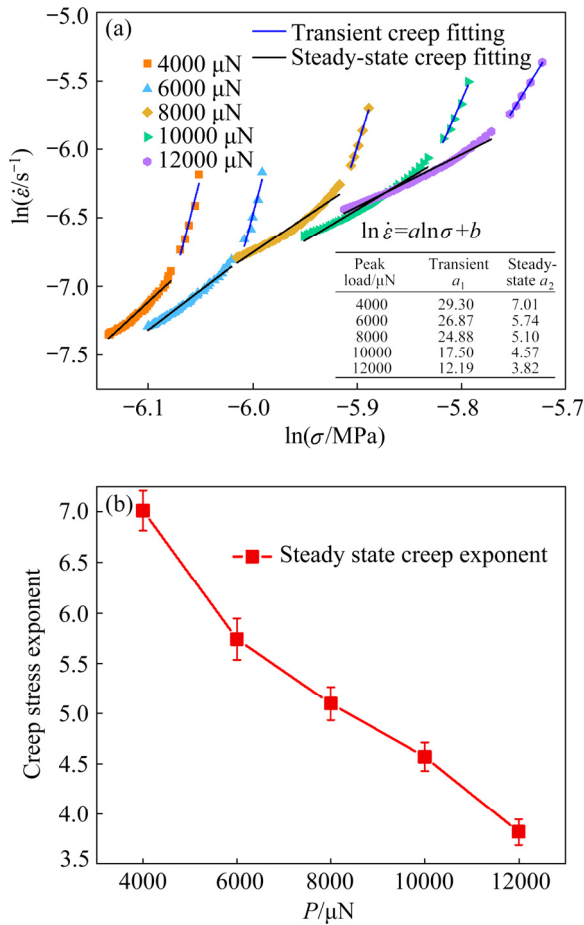


Fig. 7 Variation of stress exponent under different peak loads extracted from transient and steady-state creep stages (a), and average stress exponents and their error bars extracted from steady-state creep stage, taken as valid n under different peak loads (b)

presented the average stress exponents and their error bars under different peak loads. The creep stress exponents had apparent loading effects at room temperature, which decreased from 7.01 to 3.82 in steady-static creep as the peak loads increased. Similar to the analysis at different loading rates, it was drawn that both the strain rate and stress exponent decreased as the peak loads increased. The main reason for the phenomena could be explained as follows: as the peak load increased, the deformation of the test material increased, for the deformation resistance and the degree of work hardening to abruptly increase. Therefore, both the strain rate and creep stress exponent decreased at the holding stage. For Ni-based single crystal superalloys, LI et al [47] found that by MD simulation, as the load increased, the dislocations in the γ matrix increased

and gathered at the γ/γ' phase interface, the dislocation network at γ/γ' phase interface effectively inhibited the dislocations emitted in the γ matrix to penetrate the γ' phase and absorb the matrix dislocations to strengthen the matrix itself, which increased the structure stability. This indicated that dislocation motion and its evolution are the main deformation mechanism of Ni-based single crystal superalloys, which are consistent with those observed by ZHAO et al [48]. Moreover, all stress exponents exceeded 3 based on the nanoindentation experiments in the current study, which also indicated that the main factor causing creeping was the dislocation motion during nanoindentation under different peak loads.

The hardness and reduced modulus at each peak load were extracted in Fig. 8. Similar to different loading rates case, it can be seen that the higher peak load corresponded to a lower E_r and H . They reached a maximum of 1270.7 and 93.4 GPa at 4000 μN , and the minimum of 1071.3 and 55.4 GPa when the peak load is 12000 μN , respectively. This indicated that the indentation mechanical properties were sensitive to different peak loads in the hardness and modulus experiments of nanoindentation [39].

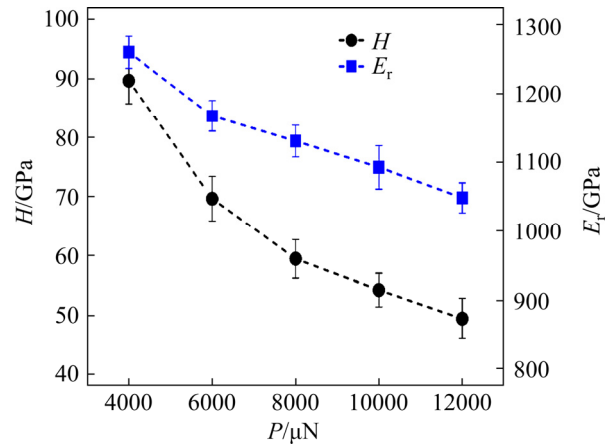


Fig. 8 Reduced modulus and hardness data for DD407 alloy under various peak loads

3.4 Comparison of applied loading rate and peak load effects on creep

The sensitivity of creep behavior to different loading rates and applied peak loads observed in this work indicated that the creep would propagate faster within the high-speed load changing regions or high peak load areas. Through our research, we found that this phenomenon was more obvious at

the nanometer scale. Therefore, the rapidly changing load and the higher sustained load on the samples led to significant differences in overall creep durability states. To quantitatively compare the effects of applied loading rate and peak load on the creep properties of DD407 alloy, a dimensionless approach, defined as the ratio of creep displacement to corresponding parameter ranges, was utilized to evaluate the temperature and load effects as [49]

$$\eta_p = \frac{h_{p1} - h_{p2}}{P_1 - P_2} \quad (11)$$

$$\eta_R = \frac{h_{R1} - h_{R2}}{R_1 - R_2} \quad (12)$$

where η_p is the ratio of creep displacement to corresponding holding peak load, and η_R is the ratio of creep displacement to corresponding loading rate. The average ratio of η_p is 1.58×10^{-3} , and the average ratio of η_R is 1.33×10^{-3} . It was shown that the dimensionless values, as calculated from Eq. (11), were higher than the values determined through Eq. (12). These observations indicated that the loading rate effect on creep properties could exceed the peak load effect.

4 Conclusions

(1) In the range of the loading rate and peak load that we tested, only primary and secondary creep stages were observed for DD407 Ni-base single crystal superalloy, which did not enter the third stage of creep, it indicated that the alloy exhibited good creep resistance during nano-indentation.

(2) Creep properties were sensitive to the loading rate and peak load, as the loading rate and peak load were increased, creep displacement increased gradually, while the creep stress exponent decreased. The creep mechanisms in both cases were dominated by dislocation based on the calculation of the stress exponent.

(3) The hardness and reduced modulus of DD407 Ni-base single crystal superalloy decreased with increasing the loading rate and peak load in nanoindentation creep tests. Moreover, through a dimensionless analysis, it was found that the effect of the dimensionless loading rate was stronger than that of dimensionless peak load on the creep properties.

Acknowledgments

The authors would like to gratefully acknowledge the financial supports from the National Natural Science Foundation of China (Nos. 11772236, 11472195).

References

- [1] WU X, DLOUHY A, EGGELER Y M, SPIECKER E, KOSTKA A, SOMSEN C, EGGELER G. On the nucleation of planar faults during low temperature and high stress creep of single crystal Ni-base superalloys [J]. *Acta Materialia*, 2018, 144: 642–655.
- [2] COAKLEY J, MA D, FROST M, DYE D, SEIDMAN D N, DUNAND D C, STONE H J. Lattice strain evolution and load partitioning during creep of a Ni-based superalloy single crystal with rafted γ' microstructure [J]. *Acta Materialia*, 2017, 135: 77–87.
- [3] XIE J, YU J J, SUN X F, JIN T. Thermodynamics analysis and precipitation behavior of fine carbide in K416B Ni-based superalloy with high W content during creep [J]. *Transactions of Nonferrous Metals Society of China*, 2015, 25(5): 1478–1483.
- [4] RAM F, LI Z, ZAEFFERER S, HAGHIGHAT S M H, ZHU Z, RABBE D, REED R C. On the origin of creep dislocations in a Ni-base, single-crystal superalloy: An ECCI, EBSD, and dislocation dynamics-based study [J]. *Acta Materialia*, 2016, 109: 151–161.
- [5] WOLLGRAMM P, BUCK H, NEUKING K, PARSA A B, SCHUWALOW S, ROGAL J, DRAUTZ R, EGGELER G. On the role of Re in the stress and temperature dependence of creep of Ni-base single crystal superalloys [J]. *Materials Science and Engineering A*, 2015, 628: 382–395.
- [6] WOLLGRAMM P, BUERGER D, PARSA A B, NEUKING K, EGGELER G. The effect of stress, temperature and loading direction on the creep behaviour of Ni-base single crystal superalloy miniature tensile specimens [J]. *Materials at High Temperatures*, 2016, 33(4/5): 346–360.
- [7] SHI D, DONG C, YANG X, SUN Y, WANG J, LIU J. Creep and fatigue lifetime analysis of directionally solidified superalloy and its brazed joints based on continuum damage mechanics at elevated temperature [J]. *Materials & Design*, 2013, 45: 643–652.
- [8] SUN W K, XU Y M, HU C Y, LIU X L. Effect of film-hole configuration on creep rupture behavior of a second generation nickel-based single crystal superalloys [J]. *Materials Characterization*, 2017, 130: 298–310.
- [9] AMINI A, YAN W Y, SUN Q P. Depth dependency of indentation hardness during solid-state phase transition of shape memory alloys [J]. *Applied Physics Letters*, 2011, 99(2): 021901.
- [10] WU W P, WEI Y, LIU P. Indentation depth-dependence of the hardness of NiTi shape memory alloy and Al single crystal: Phase transition versus plasticity [J]. *Materials Research Innovations*, 2015, 19(S5): S5-37–S5-40.
- [11] DOERNER M F, NIX W D. A method for interpreting the data from depth-sensing indentation instruments [J]. *Journal*

- of Materials Research, 1986, 1(4): 601–609.
- [12] OLIVER W C, PHARR G M. An improved technique for determining hardness and elastic modulus using load and displacement sensing indentation experiments [J]. *Journal of Materials Research*, 1992, 7(6): 1564–1583.
- [13] OLIVER W C, PHARR G M. Measurement of hardness and elastic modulus by instrumented indentation: Advances in understanding and refinements to methodology [J]. *Journal of Materials Research*, 2004, 19(1): 3–20.
- [14] HASEEB A, RAHMAN A Z M S, CHIA P Y. Nanoindentation creep on, Cu₆Sn₅ and (Cu,Ni)₆Sn₅ intermetallic compounds grown in electrodeposited multilayered thin film [J]. *Journal of Materials Science: Materials in Electronics*, 2018, 29(2): 1258–1263.
- [15] MA Y, PENG G J, WEN D H, ZHANG T H. Nanoindentation creep behavior in a CoCrFeCuNi high-entropy alloy film with two different structure states [J]. *Materials Science and Engineering A*, 2015, 621: 111–117.
- [16] PHANI P S, OLIVER W C. A direct comparison of high temperature nanoindentation creep and uniaxial creep measurements for commercial purity aluminum [J]. *Acta Materialia*, 2016, 111: 31–38.
- [17] LI Y, FANG X F, LU S Y, YU Q M, HOU G H, FENG X. Effects of creep and oxidation on reduced modulus in high-temperature nanoindentation [J]. *Materials Science and Engineering A*, 2015, 678: 65–71.
- [18] LEE D H, SEOK M Y, ZHAO Y, CHOI I C, HE J, LU Z, SUH J Y, RAMAMURTY U, KAWASAKI M, LANGDON T G, JANG J I. Spherical nanoindentation creep behavior of nanocrystalline and coarse-grained CoCrFeMnNi high-entropy alloys [J]. *Acta Materialia*, 2016, 109: 314–322.
- [19] LI H, NGAN A H W. Size effects of nanoindentation creep [J]. *Journal of Materials Research*, 2004, 19(2): 513–522.
- [20] WU J L, PAN Y, PI J H. Nanoindentation mechanical properties of indium-alloyed Cu-based bulk metallic glasses [J]. *Journal of Materials Engineering and Performance*, 2014, 23(2): 486–492.
- [21] MA Z, LONG S, PAN Y, ZHOU Y. Loading rate sensitivity of nanoindentation creep in polycrystalline Ni films [J]. *Journal of Materials Science*, 2008, 43(17): 5952–5955.
- [22] PEREZ C J, ALVAREZ V A, VAZQUEZ A. Creep behaviour of layered silicate/starch–polycaprolactone blends nanocomposites [J]. *Materials Science and Engineering A*, 2008, 480(1/2): 259–265.
- [23] WANG J, GUO W, GUO J, LU S. The effects of stress triaxiality, temperature and strain rate on the fracture characteristics of a nickel-base superalloy [J]. *Journal of Materials Engineering and Performance*, 2016, 25(5): 2043–2052.
- [24] WANG J, GUO W G, SU Y, ZHOU P, YUAN K. Anomalous behaviors of a single-crystal nickel-base superalloy over a wide range of temperatures and strain rates [J]. *Mechanics of Materials*, 2016, 94: 79–90.
- [25] WANG F, HUANG P, XU K. Strain rate sensitivity of nanoindentation creep in polycrystalline Al film on silicon substrate [J]. *Surface and Coatings Technology*, 2007, 201(9–11): 5216–5218.
- [26] HERRING C. Diffusional viscosity of a polycrystalline solid [J]. *Journal of Applied Physics*, 1950, 21(5): 437–445.
- [27] LI J C M. Physical chemistry of some microstructural phenomena [J]. *Metallurgical Transactions A*, 1978, 9(10): 1353–1380.
- [28] LUETHY H, WHITE R A, SHERBY O D. Grain boundary sliding and deformation mechanism maps [J]. *Materials Science and Engineering*, 1979, 39(2): 211–216.
- [29] GONG P, JIN J, DENG L, WANG S, GU J, YAO K, WANG X. Room temperature nanoindentation creep behavior of TiZrHfBeCu (Ni) high entropy bulk metallic glasses [J]. *Materials Science and Engineering A*, 2017, 688: 174–179.
- [30] GEORGIPOULOS P, KONTOU E, CHRISTOPOULOS A. Short-term creep behavior of a biodegradable polymer reinforced with wood-fibers [J]. *Composites (Part B): Engineering*, 2015, 80: 134–144.
- [31] ZHU X Y, LIU X J, ZENG F, PAN F. Room temperature nanoindentation creep of nanoscale Ag/Fe multilayers [J]. *Materials Letters*, 2010, 64(1): 53–56.
- [32] SUN W K, XU Y M, HU C Y, LIU X L. Effect of film-hole configuration on creep rupture behavior of a second generation nickel-based single crystal superalloys [J]. *Materials Characterization*, 2017, 130: 298–310.
- [33] NORTHWOOD D O, SMITH I O. Internal and effective stresses in the steady-state creep of polycrystalline cadmium at 0.5 T_m [J]. *Physica Status Solidi (A)*, 1986, 98(1): 163–169.
- [34] RAMAN V, BERRICHE R. An investigation of the creep processes in tin and aluminum using a depth-sensing indentation technique [J]. *Journal of Materials Research*, 1992, 7(3): 627–638.
- [35] ARICÒ A S, BRUCE P, SCROSATI B, TARASCON J M, SCHALKWIJK W V. Nanostructured materials for advanced energy conversion and storage devices [J]. *Nature Materials*, 2005, 4(5): 366–377.
- [36] LU K, LU L, SURESH S. Strengthening materials by engineering coherent internal boundaries at the nanoscale [J]. *Science*, 2009, 324(5925): 349–352.
- [37] TANG C A, LIU H, LEE P, TSUI Y, THAM L. Numerical studies of the influence of microstructure on rock failure in uniaxial compression—Part I: Effect of heterogeneity [J]. *International Journal of Rock Mechanics and Mining Sciences*, 2000, 37(4): 555–569.
- [38] SCHWAIGER R, MOSER B, DAO M, CHOLLACOOP N, SURESH S. Some critical experiments on the strain-rate sensitivity of nanocrystalline nickel [J]. *Acta Materialia*, 2003, 51(17): 5159–5172.
- [39] YANG S, ZHANG Y W, ZENG K. Analysis of nanoindentation creep for polymeric materials [J]. *Journal of Applied Physics*, 2004, 95(7): 3655–3666.
- [40] MARQUES V M F, WUNDERLE B, JOHNSTON C, GRANT P S. Nanomechanical characterization of Sn–Ag–Cu/Cu joints—Part 2: Nanoindentation creep and its relationship with uniaxial creep as a function of temperature [J]. *Acta Materialia*, 2013, 61(7): 2471–2480.
- [41] WANG C L, LAI Y H, HUANG J C, NIEH T G. Creep of nanocrystalline nickel: A direct comparison between uniaxial and nanoindentation creep [J]. *Scripta Materialia*, 2010, 62(4): 175–178.
- [42] CARMINE M, FABRIZION N, EMANUELE S, FRANCO F.

- Analysis of fatigue damage in shape memory alloys by nanoindentation [J]. *Materials Science and Engineering A*, 2017, 684: 335–343.
- [43] MUKHERJEE A K, BIRD J E, DORN J E. Experimental correlations for high-temperature creep [C]//Congress of American Society for Metals. Berkeley, USA: University of California, 1968.
- [44] MCDUGALL J, CHOI S, BIELER T R, SUBRAMANIAN K N, LUCAS J P. Quantification of creep strain distribution in small crept lead-free in-situ composite and non composite solder joints [J]. *Materials Science and Engineering A*, 2000, 285(1/2): 25–34.
- [45] LÜETHY H, WHITE R A, SHERBY O D. Grain boundary sliding and deformation mechanism maps [J]. *Materials Science and Engineering*, 1979, 39(2): 211–216.
- [46] BLUM W, ZENG X H. A simple dislocation model of deformation resistance of ultrafine-grained materials explaining Hall–Petch strengthening and enhanced strain rate sensitivity [J]. *Acta Materialia*, 2009, 57(6): 1966–1974.
- [47] LI N L, WU W P, NIE K. Molecular dynamics study on the evolution of interfacial dislocation network and mechanical properties of Ni-based single crystal superalloys [J]. *Physics Letters A*, 2018, 382(20): 1361–1367.
- [48] ZHAO X H, HUANG Z H, SUN Y J, XU H B. Creep behavior and microstructure evolution of directionally solidified superalloy IC10 at high temperature [J]. *Transactions of Nonferrous Metals Society of China*, 2006, 16(S2): s122–s126.
- [49] HU J H, LI Y P, CHEN W J, ZHAO B, YANG D Q. Effects of temperature and stress on creep properties of ethylene tetrafluoroethylene (ETFE) foils for transparent buildings [J]. *Polymer Testing*, 2017, 59: 268–276.

加载速率和峰值载荷对 DD407 镍基单晶高温合金 纳米压痕蠕变行为的影响

张震男¹, 李云丽², 吴文平^{1,3}

1. 武汉大学 土木建筑工程学院 工程力学系, 武汉 430072;
2. 武汉工程大学 土木工程与建筑学院, 武汉 430074;
3. 武汉大学 水利水电工程科学国家重点实验室, 武汉 430072

摘要: 在加载速率 500~6000 uN/s 和峰值载荷 4000~12000 uN 的条件下进行纳米压痕蠕变实验, 研究 DD407 镍基单晶高温合金在室温下的蠕变行为。结果表明: DD407 镍基单晶高温合金具有良好的蠕变抗力性能, 但其蠕变性能对加载速率和峰值载荷敏感。依据 Findley 模型, 得到拟合的蠕变参数随着加载速率和峰值载荷的增加而显著增加, 并通过计算蠕变应力指数得到合金的蠕变机理由位错控制。此外, 在纳米压痕蠕变实验中发现 DD407 合金的硬度和模量随着加载速率和峰值载荷的增加而降低, 并通过无量纲分析得到加载速率对蠕变性能的影响大于峰值载荷对蠕变性能的影响。

关键词: DD407 镍基单晶高温合金; 纳米压痕; Findley 模型; 蠕变; 应力指数

(Edited by Xiang-qun LI)